A replicable and generalizable neuroimaging-based indicator of pain sensitivity across individuals

Authors: Li-Bo Zhang[1,2,3], Xue-Jing Lu[1,2], Hui-Juan Zhang[1,2], Zhao-Xing Wei[2,4], Ya-Zhuo Kong[2,4], Yi-Heng Tu[1,2], Gian Domenico Iannetti[3,5], Li Hu[1,2,*]

Affiliations:

[1]CAS Key Laboratory of Mental Health, Institute of Psychology, Chinese Academy of Sciences, 100101, Beijing, China;

[2]Department of Psychology, University of Chinese Academy of Sciences, 100049, Beijing, China;

[3]Neuroscience and Behaviour Laboratory, Italian Institute of Technology, 00161, Rome, Italy;

[4]CAS Key Laboratory of Behavioral Science, Institute of Psychology, Chinese Academy of Sciences, 100101, Beijing, China;

[5]Department of Neuroscience, Physiology and Pharmacology, University College London, WC1E 6BT, London, UK.

*Corresponding author. Email: huli@psych.ac.cn

Abstract

Developing neural indicators of pain sensitivity is crucial for revealing the neural basis of individual differences in pain and advancing individualized pain treatment. To identify reliable neural indicators of pain sensitivity, we leveraged five large and diverse functional magnetic resonance imaging (fMRI) datasets (total N=1010). We found replicable and generalizable correlations between pain-evoked fMRI responses and pain sensitivity for laser heat, contact heat, and mechanical pains. These fMRI responses correlated more strongly with pain sensitivity than with tactile, auditory, and visual sensitivity. Moreover, we developed a machine learning model that accurately predicted not only pain sensitivity but also pain relief from different analgesic treatments. Notably, these findings were influenced considerably by sample sizes, requiring >200 for univariate correlation analysis and >150 for multivariate machine learning modelling. Altogether, we demonstrate the validity of decoding pain sensitivity and predict analgesic effects using fMRI responses, offering clinical promise in tailoring individualized pain treatments.

Keywords: pain sensitivity, individual differences, functional magnetic resonance imaging (fMRI), sample size, machine learning, analgesic effects

Introduction

Pain sensitivity varies widely across individuals[1]. The same nociceptive stimulus may be intolerably painful for someone, yet barely perceivable by another. What neural activity encodes such dramatic variability of pain sensitivity? This is a fundamental question in pain neuroscience. Understanding this is important not only for objectively measuring pain sensitivity, but also for improving the diagnosis and treatment of clinically relevant pain. High pain sensitivity is a risk factor for chronic pain[2–4] – a condition that afflicts more than 20% of adults[5,6]. Identifying neural indicators of pain sensitivity could therefore aid in screening high-risk individuals for chronic pain and developing individualized pain treatment strategies[7–9].

Numerous previous studies have attempted to find neural indicators of pain sensitivity with non-invasive neuroimaging techniques like functional magnetic resonance imaging (fMRI)[10–14]. However, three key issues remain not well-addressed as of now. First and foremost, it is still subject to heated debate whether pain-evoked brain activations can serve as neural indicators of pain sensitivity. Painful stimuli consistently activate a series of brain areas such as the primary somatosensory cortex (S1), secondary somatosensory cortex (S2), anterior cingulate cortex (ACC), insula, thalamus, and prefrontal cortex (PFC)[15,16]. An early small (N=17) but seminal study linked larger pain-evoked blood oxygen level dependent (BOLD) responses in these areas with higher pain sensitivity[10]. Yet, a recent study with a large sample size (N=101) found that no single brain area significantly correlated with pain sensitivity[11]. With a slightly larger sample size (N=124), another recent study observed weak but significant correlations between pain-evoked BOLD responses and pain sensitivity[17]. These discrepant findings may exemplify the replication crisis in empirical sciences[18–21]. One critical cause of non-replicability is sample size[22]. Recent studies suggest that a sample size of ~100 in functional neuroimaging studies may be insufficient to reliably reveal the association between BOLD responses and behaviors at the inter-individual level[23,24], especially when the true correlation is small[17,25].

Another unresolved issue is whether pain-evoked brain responses selectively track pain sensitivity rather than modality-independent stimulus factors[26]. Previous studies have

shown that pain-evoked neural responses can be evoked by nonpainful but equally salient tactile, auditory, and visual stimuli[27–30], implying that these responses are not pain selective. However, recent studies have found some small brain regions[31,32] and brain activity patterns[33,34] that respond more to painful stimuli than to nonpainful stimuli, suggesting potentially preferential encoding of pain in the brain. Notably, rarely have these studies quantitatively examined whether certain brain region or activity pattern correlates with individual differences in pain and other modalities alike at the *between-individual* level. Instead, they have mainly focused on whether pain-evoked brain responses selectively track pain experience at the *within-individual* level. As a result, previous studies have yet to provide a conclusive answer to the question of whether there are selective neural indicators of pain sensitivity.

The third issue concerns the transferability of neural indicators of pain sensitivity. Such neural indicators have been primarily developed to assess pain sensitivity objectively[26,35]. Predicting medication responses is also an oft-mentioned purpose of identifying neural indicators[26,36,37]. Nevertheless, it has not been adequately evaluated whether neural indicators of pain sensitivity can be transferred to predict outcomes of pain treatments. Given the close link between pain modulation system and pain sensitivity[38,39], there is a plausible basis for neural indicators of pain sensitivity to predict analgesic effects. It thus holds great potential to investigate the transferability of neural indicators of pain sensitivity to predict pain relief, which can foster individualized pain treatments.

To address these issues, we leveraged five large and diverse fMRI datasets (total N=1010) from three countries (China, US, and South Korea), where healthy participants received various types of painful stimuli: laser heat pain in Datasets 1 and 2[14], mechanical pain in Dataset 3[40], contact heat pain in Datasets 4[17] and 5[41] (see Table S1 for a brief summary of each dataset). We aimed to answer four key questions (Figure 1A): (1) Do pain-evoked BOLD responses reflect pain sensitivity across individuals? (2) If so, is this correlation selective to the pain modality? (3) Can we develop a machine learning (ML) model that is versatile enough to accurately predict pain sensitivity and pain relief? (4) Which sample size is needed to reliably decode pain sensitivity from BOLD responses? First, we

correlated pain-evoked BOLD responses with pain sensitivity and tested the replicability and generalizability of the correlation with Datasets 1~3 (N=794). Subsequently, we examined whether the correlation between BOLD responses and sensory sensitivity differs between pain and nonpain modalities with Datasets 1&2 (N=399), where participants also received nonpainful tactile, auditory, and visual stimuli (Figure 1B). Next, we built a multivariate ML model, named the Neuroimaging-based Indicator of Pain Sensitivity (NIPS) model, to predict pain sensitivity using pain-evoked BOLD responses. We evaluated NIPS's performance with Datasets 1&2, examined its generalizability across various pain types and diverse populations, and assessed its predictive power on analgesic effects with three large external datasets, i.e., Datasets 3~5 (total N=608). Finally, we systematically examined the influence of sample sizes on the ability to reliably detect the univariate correlation between BOLD responses and pain sensitivity and the performance of multivariate predictive models.

Results

BOLD responses reliably reflect pain sensitivity

We utilized Datasets 1~3 to examine whether pain-evoked BOLD responses reliably reflect inter-individual pain sensitivity. In Datasets 1&2, participants received and rated sensory stimuli of four modalities (painful, tactile, auditory, and visual) with two levels of physical intensity (low and high)[14]; in Dataset 3, participants received mechanical pain stimuli with three levels of physical intensity (6kg/cm^2, 7kg/cm^2, and 8kg/cm^2)[40]. Dataset 1 delivered laser heat pain stimuli of 3.0J and 3.5J, and Dataset 2 delivered stimuli of 3.5J and 4.0J. To make full use of the large sample size, we pooled data from the 3.5J condition (N=399) and tested the correlation between BOLD responses and pain sensitivity. We then assessed the replicability of the finding from this pooled dataset with data from the 3.0J condition in Dataset 1, the 4.0J condition in Dataset 2, and the mechanical pain data from Dataset 3. Finally, we explored the effect of sample sizes on our findings by generating bootstrapped samples from Datasets 1~3[42]. Note that Dataset 3 was originally collected to investigate placebo analgesia[40]. Here we utilized only the fMRI data in the control condition where no placebo cream was applied.

In Datasets 1&2, 10 laser heat pain stimuli per condition were delivered to participants. We quantified pain sensitivity as the mean pain rating for the 10 stimuli. As in previous studies[1,11,17], we observed considerable inter-individual variability of pain sensitivity even though the painful stimuli had identical physical intensity. Pain sensitivity ranged from 0.8 to 9.9 (mean±standard deviation [SD]: 4.54±1.72; Figure 2A and Table S4), covering almost the entire range of the 0 (‘‘no sensation’’) ~ 10 (‘‘the strongest sensation imaginable”) rating scale. Painful stimuli also activated a wide range of typically pain-related brain areas, including the S1, S2, ACC, insula, and thalamus (Figure 1C).

Importantly, we found significant Pearson’s correlations between pain-evoked BOLD responses and pain sensitivity across individuals (Figure 2A; p(FDR)<0.05, the same hereafter). The majority of the correlations were positive, including the S1, S2, ACC, insula, thalamus, precentral gyrus, supplementary motor area, precuneus, cerebellum, and the like. Negative correlations with pain sensitivity were only observed in a few areas, and the

correlation coefficients were generally smaller than those of positive correlations. To test the robustness of this finding, we also conducted Spearman's rank correlation analysis. A similar significant correlation pattern was found (Figure S1A; Pearson's r between the two unthresholded correlation maps=0.958). In the analyses above, we accounted for head motion with the classical six motion parameters. To further control the potential influence of head motion, we regressed out from the BOLD signals the six motion parameters, their first derivatives, and squares of the motion parameters and first derivatives[43]. Still, the significant correlation pattern resembled that of our original finding (Figure S1B; Pearson's r between the two unthresholded correlation maps=0.936), suggesting a negligible influence of head motion on our finding.

We then examined whether our finding could be replicated with the same dataset and generalized to other datasets. In both the 3.0J condition in Dataset 1 and the 4.0J condition in Dataset 2, significant correlations were present in a series of brain areas (Figure 2B). However, fewer areas showed significant correlations in these two conditions, which could be associated with their sample sizes being only half of the pooled 3.5J condition (~200 vs. ~400), thereby reducing the statistical power to detect true effects. In Dataset 3, we also found significant correlations between pain-evoked BOLD responses and pain sensitivity in all three physical intensity conditions (Figure 2C). Notably, the largest correlation was consistently around 0.4 in Datasets 1~3. Fewer areas showed significant correlations as the physical intensity decreased. One plausible explanation could be that painful stimuli of low intensity, such as 6kg/cm^2, might not reliably induce pain sensation, potentially resulting in a poor signal-to-noise ratio of the BOLD responses. Indeed, in the 6kg/cm^2 condition, 101 participants (27.2%) had a mean pain rating <0.014, which was defined as "barely detectable pain". In agreement with laser heat pain in Datasets 1&2 and mechanical pain in Dataset 3, a previous study analyzing Dataset 4, where contact heat pain stimuli were delivered, also observed significant correlations between BOLD responses and pain sensitivity[17]. Consistent findings in these datasets demonstrate not only the replicability of the correlation between BOLD responses and pain sensitivity, but also the generalizability of the correlation across different types of painful stimuli in diverse populations. To directly test whether classical pain-related areas encode pain sensitivity, we extracted mean

signals from the S1, S2, ACC, insula, and thalamus in Datasets 1~3 using anatomically defined masks. Significant correlations were observed in most of these regions of interest (ROI) except when the physical intensity was low (i.e., 6kg/cm^2) in Dataset 3 (Table S5&S6).

Given the inconsistent findings in previous studies with smaller sample sizes[10,11,17], we systematically investigated the potential influence of sample size on the BOLD responses-pain sensitivity correlation in the 3.5J condition from Datasets 1&2. Briefly, we sampled with replacement 100~400 participants (in steps of 10) from Datasets 1&2, repeated the process 100 times, and estimated the sample size needed to detect a significant correlation in every voxel with a probability ≥0.8[44] (see **Methods** for details). The sample size needed for different voxels varied greatly across the brain (Figure 3A). For voxels that showed significant correlations, the median sample size needed was 280, with an SD=78 (Figure 3A). To specifically focus on the pain-related ROIs, we also estimated the probability of obtaining significant correlations for the S1, S2, ACC, insula, and thalamus (Figure 3B). With α=0.01, the S2 required the smallest sample size (~150) to reach significance with a probability of 0.8; with α=0.001, the S2 required a sample size of ~220. Importantly, we also obtained similar findings in Dataset 3. In this independent dataset, a sample size of 270 was needed for half of the significant voxels to be detected with a probability ≥0.8 (Figure 3C). ROI analysis suggested that the insula required the smallest sample size of ~180 and ~240 to reach significance with a probability of 0.8, with α=0.01 and 0.001 respectively (Figure 3D). These findings in independent datasets converge to reaffirm that the sample size had an enormous influence on the ability to detect significant correlations between BOLD responses and pain sensitivity, and more than 200 participants would be needed to reliably detect their correlations.

BOLD responses differentially reflect pain sensitivity and nonpain sensitivity

Having shown that BOLD responses reliably reflect pain sensitivity, we then examined in Datasets 1&2 whether the correlation is selective to the pain modality by correlating tactile, auditory, and visual stimuli-evoked BOLD responses with the corresponding sensory sensitivity. We also compared the correlation coefficients between modalities[45]. Moreover,

to rule out the potential confounding of sensitivity differences between modalities, we selected participants who had no significant sensitivity differences between modalities (see **Methods** for details) and correlated BOLD signals with sensory sensitivity in these participants with matched pain and nonpain sensitivity.

In agreement with previous findings[28], brain regions activated by tactile, auditory, and visual stimuli were highly similar to those activated by painful stimuli (Figure 1C). However, Pearson's correlational results exhibited distinct patterns across modalities. BOLD responses evoked by high intensity tactile stimuli correlated significantly with tactile sensitivity in several brain areas (Figure 4A), while significant correlations only occurred in some small and scattered brain areas for high intensity auditory and visual stimuli (Figure 4B&C). These results remained largely the same if Spearman's rho was computed rather than Pearson's r (Figure S2). In the low intensity conditions, however, only a few brain areas showed significant positive correlations for all three nonpain modalities (Figure S3). As the stimulus intensity seemed to exert substantial influences on the results, we focused on the high intensity conditions hereafter. To avoid the imager's fallacy[46], we then directly compared correlation coefficients between pain and nonpain modalities. For the pain vs. touch comparison, significant differences in correlation coefficients were observed in some small areas, notably in the S1, precentral gyrus, and supplementary motor area (Figure 4D). For pain vs. audition and pain vs. vision comparisons, significant differences were found in many more areas, covering typical pain-related areas, such as the S1, S2, ACC, insula, and thalamus (Figure 4D).

However, the foregoing findings might be confounded by sensitivity differences between modalities. Indeed, there were significant differences in mean ratings (i.e., sensitivity) among the four modalities ($F(3,1194)=117.295$, $p<0.001$, partial $\eta^2=0.228$). Post-hoc tests revealed larger tactile ratings than painful and auditory ratings, and larger visual ratings than painful, tactile, and auditory ratings (Figure S4, Table S7). To equalize sensitivity between modalities, we adopted a within-individual sensitivity matching approach, selecting participants whose 95% confidence interval of the mean difference between pain and nonpain sensitivity contained 0[33]. With this approach, we selected 192 participants for

the pain-touch matching, 171 participants for the pain-audition matching, and 147 participants for the pain-vision matching. In the matched samples for pain-touch and pain-audition, we found that pain-evoked BOLD signals correlated with pain sensitivity in numerous areas (Figure 5A&B). In the matched samples for pain-vision, we observed significant correlations with pain sensitivity in several small areas like the thalamus and supplementary motor area (Figure 5C). By contrast, in all three matched samples, BOLD responses in few, if any, areas showed significant correlations with tactile, auditory, and visual sensitivity (Figure 5A~C). Directly comparing correlation coefficients between modalities in these matched samples showed a diverse array of regions had greater correlations with pain sensitivity than with nonpain sensitivity (Figure 5D). Altogether, these findings demonstrate that there are quantitative differences in the correlation between BOLD responses and pain vs. nonpain sensitivity.

NIPS accurately predicts sensitivity to various pains in diverse populations

We next developed a neuroimaging-based ML model (i.e., NIPS) to predict pain sensitivity across individuals. We first split randomly the pooled 3.5J data in Datasets 1&2 into a Discovery Set (N=199) and a Holdout Test Set (N=200). NIPS was developed with data in the Discovery Set and tested in the Holdout Test Set. To ensure NIPS's generalizability, we assessed its predictive power in external Dataset 3 (N=395) and Dataset 4 (N=124). As in the univariate analyses, we also examined the effect of sample sizes on NIPS's performance.

To build the model, we used the least absolute shrinkage and selection operator-based principal component regression (LASSO-PCR; Figure 6A). In the Discovery Set, NIPS accurately predicted pain sensitivity with its 5-fold cross-validated performance as follows: $r=0.531$, $p<0.0001$, $R^2=0.242$ (Figure 6B). NIPS also performed well in the Holdout Test Set: $r=0.496$, $p<0.0001$, $R^2=0.237$ (Figure 6B). NIPS thus could explain >20% of the variance of pain sensitivity in both the Discovery Set and Holdout Test Set. Even though NIPS was built based on the data from the 3.5J condition in the Discovery Set, it was also able to predict pain sensitivity in the 3.0J condition (N=101; $r=0.404$, $p<0.0001$, $R^2=0.146$) and the 4.0J condition (N=99; $r=0.489$, $p<0.0001$, $R^2=0.229$) in the Holdout Test Set. To

compare the performance of NIPS with other well-established pain prediction models, we applied the Neurological Pain Signature (NPS)[36] and Stimulus Intensity Independent Pain Signature-1 (SIIPS1)[37] to the Holdout Test Set. Both NPS and SIIPS1 significantly predicted pain sensitivity ($r=0.336$, $p<0.0001$ and $r=0.386$, $p<0.0001$, respectively) (Figure 6C). A simple model based on the pain-related activation pattern derived from a term-based meta-analysis with neurosynth (Neurosynth "pain" model) also predicted pain sensitivity in the Holdout Test Set ($r=0.224$, $p=0.001$) (Figure 6C). Notably, NPS, SIIPS, and Neurosynth "pain" all had significantly smaller predictive power compared with NIPS: (1) NIPS vs. NPS: $t=2.819$, $p=0.005$; (2) NIPS vs. SIIPS: $t=2.275$, $p=0.024$; (3) NIPS vs. Neurosynth "pain": $t=4.027$, $p<0.0001$. Altogether, these findings demonstrate that NIPS can accurately predict pain sensitivity, explaining more than 20% of the variance of pain sensitivity across individuals.

NIPS was developed using BOLD responses evoked by laser heat pain. To examine its generalizability, we then used it to predict mechanical pain sensitivity in Dataset 3 and contact heat pain sensitivity in Dataset 4. In Dataset 3, NIPS significantly predicted mechanical pain sensitivity in all three conditions: (1) the 8kg/cm^2 condition: $r=0.274$, $p<0.0001$; (2) the 7kg/cm^2 condition: $r=0.217$, $p<0.0001$; (3) the 6kg/cm^2 condition: $r=0.292$, $p<0.0001$ (Figure 6D). Likewise, NIPS significantly predicted contact heat pain sensitivity in Dataset 4: $r=0.323$, $p=0.0003$ (Figure 6D). Interestingly, this correlation was close to what the original authors of Dataset 4 observed ($r=0.252$) in their own study, where a specific model was built to predict contact heat pain sensitivity[17]. These results suggest that NIPS is generalizable to other pain types apart from laser heat pain.

To examine the effect of sample size on the model performance, we also resampled data (training sample size: 20 to 300, in steps of 5) in the pooled 3.5J condition in Datasets 1&2. Note that 5-fold cross-validation was adopted to assess the model performance. Therefore, for a sample of 100 participants, the training sample size (the abscissa in Figure 6E) is 80. When the training sample size was smaller than or equal to 70 (i.e., total sample size ≈88), NIPS's performance was very poor, even worse than a simple mean prediction ($R^2<0$), and varied dramatically. When the training sample size was around 100 (i.e., 95, 100, or 105),

the R^2 of NIPS was approximately 0.06. Interestingly, this estimate was very close to what Gim et al[17] found with a training sample size of 99 (model performance: r=0.252, R^2=0.064). Nevertheless, with such a sample size, NIPS's performance still varied substantially. The performance stabilized only after the training sample size reached 120 (i.e., total N=150) and then R^2 kept increasing with the training sample size. These findings suggest that a large sample size (>150) is needed to build a well-performing and robust pain prediction model.

NIPS is a distributed pattern predictive of analgesic effects

Having tested NIPS's performance, we then attempted to understand what it represents. We first used virtual lesion to examine which brain areas contributed to NIPS's predictive power[47]. We then interpreted the weight map of NIPS with neuromaps[48]. We finally tested NIPS's transferability to predict the analgesic effects of placebo in Dataset 3 and neuromodulation in Dataset 5.

The weight map of NIPS exhibited widespread positive and negative weights across the entire brain (Figure 7A, p(FDR)<0.05 for all voxels passing the strict 0.5/-0.5 threshold). Notably, pain-related areas typically had positive weights, such as the ACC, insula, thalamus, and cerebellum, while the PFC and occipital cortex showed negative weights. To explore which areas were more important, we parcellated the brain according to the Automatic Anatomical Labeling template[49], removed (i.e., "virtually lesioned") each area, and refitted the predictive model without the corresponding area. We found that none of the areas was practically indispensable for NIPS's performance (Figure 7B; see supplemental data file for complete results). However, keeping only one area while removing all others greatly reduced NIPS's performance (Figure S5). Taken together, these findings suggest that information about pain sensitivity is represented in a distributed neural system, rather than local and isolated regions[50].

To further understand what NIPS represents, we explored its neurotransmitter receptor profiles with neuromaps[48]. We only observed a significant spatial correlation between the weight map of NIPS and the spatial distribution of the mu-opioid receptor (MOR) (r=0.405,

p_{spin}(FDR)=0.034; Figure 7C), indicating that NIPS may be associated with analgesic effects due to the key role of MOR in the pain modulation system[51]. To specifically test the hypothesis and evaluate NIPS's transferability, we then applied NIPS to predict analgesic effects using Datasets 3&5. Dataset 3 was originally collected to investigate placebo analgesia[40]. We previously utilized the fMRI data in the control condition in Dataset 3 to test the generalizability of NIPS (Figure 6E). We now subtracted BOLD responses and mean pain ratings in the placebo condition from the control condition to quantify the placebo effect. NIPS significantly predicted the magnitude of placebo analgesia: (1) the 8kg/cm^2 condition: r=0.205, p<0.0001; (2) the 7kg/cm^2 condition: r=0.167, p=0.002; (3) the 6kg/cm^2 condition: r=0.204, p<0.0001 (Figure 7D). Dataset 5 was collected to study the analgesic effect of transcutaneous electrical nerve stimulation (TENS) with a pretest-treatment-posttest design[41]. To quantify the analgesic effect, we subtracted BOLD responses and mean pain ratings in the posttest from those in the pretest. We also found a significant correlation between the model predictions and real pain reductions (r=0.254, p=0.015; Figure 7D). To account for the influence of baseline pain ratings (control condition in Dataset 3 and pretest condition in Dataset 5), we also conducted partial correlation analyses controlling baseline pain ratings. Still, predicted analgesic effects were significantly correlated with real pain reductions: (1) the 8kg/cm^2 condition in Dataset 3: partial r=0.181, p=0.0005; (2) the 7kg/cm^2 condition in Dataset 3: partial r=0.131, p=0.015; (3) the 6kg/cm^2 condition in Dataset 3: partial r=0.107, p=0.041; (3) Dataset 5: partial r=0.238, p=0.023. These findings converged to support the proposition that NIPS predicts, at least partly, analgesic effects from pain treatments.

Discussion

With five large and diverse fMRI datasets, we systematically examined the relationship between pain-evoked BOLD responses and pain sensitivity across individuals. We obtained four major findings. First, there were replicable and generalizable correlations between pain-evoked BOLD responses and pain sensitivity. Second, the correlations between BOLD responses and sensory sensitivity were more evident in pain than in other modalities. Third, NIPS accurately predicted not only pain sensitivity across different pain types, but also pain relief from different pain treatments. Fourth, sample sizes had enormous impacts on assessing the relationship between BOLD responses and pain sensitivity using both univariate correlation analysis and multivariate predictive modelling. Altogether, using the largest dataset on pain-evoked fMRI responses available to date, we demonstrate that pain-evoked BOLD responses can serve as replicable, generalizable, and transferable neural indicators of pain sensitivity. These findings would have profound clinical significance to help measure pain sensitivity objectively and foster individualized pain treatment.

Understanding the neural basis of variability of pain sensitivity has been a major topic in pain neuroscience[10–14,27,52–54]. Theoretically, pain-evoked BOLD responses reflect real-time neural processing of painful stimuli, thus potentially having a stronger correlation with pain sensitivity than other brain features, such as grey matter volume[52], cortical thickness[54], and resting-state functional connectivity[12,13]. Indeed, task fMRI data do improve the prediction of cognitive traits compared with resting-state fMRI data[55,56]. However, it is still highly controversial whether pain-evoked BOLD responses can reliably encode pain sensitivity, since inconsistent findings were obtained in different groups even when the sample size (≈100) seemed large[11,17]. Leveraging five large and diverse datasets, we found that pain-evoked BOLD responses reliably correlated with pain sensitivity. This correlation was robust regardless of whether parametric or nonparametric statistical methods were employed, replicable in multiple datasets with different stimulus intensities, and generalizable across different pain types in diverse populations. In agreement with previous studies[10,15,17], typical pain-related areas were also among the areas encoding pain sensitivity. We thus provided compelling evidence that, given sufficiently large sample

sizes, pain sensitivity could be indexed from BOLD responses to pain, which is consistent in principle with previous studies showing the ability of pain-evoked electrophysiological responses to encode pain sensitivity[27,53].

We also developed NIPS to predict pain sensitivity from pain-evoked BOLD responses. With multiple independent datasets, we confirmed that NIPS has good predictive performance. Cross-validation and testing in the Holdout Test Set demonstrated that NIPS explained more than 20% of the variance of pain sensitivity (Figure 6). Crucially, we tested NIPS's generalizability by applying it to mechanical pain data in Dataset 3 and contact heat pain data in Dataset 4. Although developed with laser heat pain data, NIPS exhibited significant predictive power in both datasets, demonstrating broad generalizability across different pain types. This generalizability is particularly remarkable, given the diverse backgrounds of participants in our datasets: Chinese in the Discovery and Holdout Test Sets, Americans in Dataset 3, and South Koreans in Dataset 4. NIPS thus showed extensive generalizability across ethnic groups and cultures, even though previous studies have observed ethnic and cultural differences in pain[57,58].

Given these robust and generalizable findings, why did some studies fail to find any correlation between BOLD responses and pain sensitivity? We examined two likely explanations. One is that the physical intensity of painful stimuli may be too small to evoke a clear pain sensation[59]. The power to detect correlations will be dampened if no clear pain sensation is elicited or BOLD responses are just too noisy due to insufficient physical intensity. Our results from Dataset 3 supported this explanation: fewer areas showed significant correlations with pain sensitivity as the physical intensity decreased (Figure 2C). The other explanation is that the sample size may be simply not large enough. Traditionally, neuroimaging studies have limited sample sizes[60,61], which is a crucial factor in the non-replicability of study findings[22,24]. Taking advantage of our large datasets, we systematically investigated the impact of sample size on the detectability of univariate correlations between pain-evoked BOLD signals and pain sensitivity with resampling analysis. We found that a sample size of around 200 could only detect less than 25% of the significant voxels in univariate correlation analysis (Figure 3). Similarly, sample sizes also

had a substantial influence on the predictive power of NIPS. Its predictive performance improved continuously as the sample size grew, suggesting that better models can be built with even more data[62–64]. On the other hand, the performance of NIPS varied dramatically when the sample size was small. Only when the sample size reached 150 did we observe stable predictive performance. In summary, a sample size >200 seems required for univariate correlation analysis to reveal the correlation between BOLD response and pain sensitivity, and a sample size >150 is needed to build a robust and well-performing ML model to decode pain sensitivity. This conclusion resonates with recent studies showing that a massive sample size like several hundred or even thousand is required to detect replicable brain-behavior associations[23,24,65,66].

Previous studies have shown that painful and nonpainful stimuli activate more or less the same brain regions[28,30,33], which was replicated in our study (Figure 1C), suggesting that BOLD responses may not selectively reflect pain. We did find significant correlations between nonpainful stimuli-evoked BOLD responses and corresponding sensory sensitivity (Figure 4A~C), which agrees with a recent study showing correlations between BOLD responses and auditory sensitivity[11]. However, we observed larger correlations between BOLD responses and pain sensitivity than between BOLD signals and tactile/auditory/visual sensitivity (Figure 4D), even after sensitivity differences between modalities were controlled by a matching procedure (Figure 5). Therefore, although the correlation between BOLD responses and sensory sensitivity is not unique to pain, there are quantitatively larger correlations in pain than in other sensory modalities. In other words, the brain is more capable of representing pain sensitivity. Some recent studies have identified brain areas whose activity preferentially encodes pain[31–34], but they have mainly focused on the relationship between fMRI responses and pain perception at the within-individual level. Our study thus advances this line of research by showing that fMRI responses differentially encode pain sensitivity at the between-individual level. Future research is in need to reveal the underlying mechanisms of differential encoding of pain sensitivity and nonpain sensitivity.

Crucially, the weight map of NIPS significantly correlated with the spatial distribution of MOR. Since MOR is heavily involved in pain modulation[51], we hypothesized that NIPS could be related to pain modulation as well. Directly applying NIPS to Datasets 3&5 confirmed this hypothesis: NIPS could be transferred to significantly predict analgesic effects in both datasets with different pain treatments. These findings suggest a promising clinical application of NIPS, that is, predicting analgesic effects, which fosters individualized pain treatment. Moreover, these findings bridge two types of individual differences, namely, pain sensitivity and pain relief, suggesting that pain sensitivity may be co-determined by individuals' ability to both process and modulate nociceptive information. This statement was supported by the difference in the power of predicting pain sensitivity and analgesic effects: NIPS explained more variance of pain sensitivity than the variance of analgesic effects in the same independent dataset not involved in the development of NIPS (i.e., Dataset 3). Notably, consistent with this notion, some studies discovered significant associations between pain sensitivity and conditioned pain modulation[38,39].

Despite the theoretical and clinical significance, our study has some limitations. First, we only investigated the influence of stimulus intensity and sample size on the detectability of the correlation between BOLD responses and pain sensitivity due to the nature of available datasets. Other contributing factors like sample personal characteristics and study design need to be tested in future studies. Second, while NIPS has reasonably good performance in predicting pain sensitivity, its predictive power can be further improved. As suggested by our resampling analysis, collecting even more data has the potential to boost NIPS's predictive performance[67]. Incorporating multimodal data, such as resting-state fMRI and structural MRI, in NIPS may be helpful to capture more variability of pain sensitivity, thus further improving the predictive performance[64]. Finally, participants in all datasets were healthy individuals. It thus remains to be tested whether our findings can be generalized to chronic pain patients, and it is of particular interest to test whether NIPS can predict pain relief in patient groups.

Methods

Datasets overview

We utilized five large and diverse fMRI datasets that had been published recently to study other research questions (Figure 1A). We collected Datasets 1, 2, and 5 using E-Prime (ver. 2.0, PST Inc.) on our own in China. Datasets 3 and 4 were collected using Matlab (ver. 2018b) in the US and South Korea, respectively, and kindly shared by the original authors[17,40]. In Datasets 1 and 2, participants received laser pain, electro-tactile, auditory, and visual stimuli[14]. Dataset 3 was originally collected to investigate the neural underpinnings of placebo analgesia[40]. The researchers delivered both contact heat pain and mechanical pain stimuli to participants, but used contact heat pain stimuli to induce placebo analgesia by conditioning. To avoid potential influence of the placebo induction on the neural processing of contact heat pain, we analyzed data only for the mechanical pain stimuli in the placebo and control conditions, and discarded data with contact heat pain stimuli. Instead, we used data with contact heat pain stimuli from Dataset 4[17], where no additional interventions like placebo were introduced. Dataset 5 also used contact heat pain stimuli, and was from a study aiming to reveal the spino-cortical mechanisms of TENS-induced analgesia[41]. In Datasets 1~4, the physical intensity of painful stimuli was fixed. In Dataset 5, however, the physical intensity was adjusted individually for each participant. Therefore, we did not include this dataset in most analyses, but only applied NIPS to it to test whether NIPS could predict pain relief. We summarized basic information for these five datasets in Table S1.

Participants

Dataset 1 included 212 participants. One participant did not provide the necessary demographic information. For the rest 211 participants, there were 135 females, aged 21.5 ± 4.2 years (Mean ± SD). Dataset 2 had 187 participants. There was also one participant who did not provide the demographic information. For the rest 186 participants, there were 103 females, aged 21.0 ± 3.3 years. Dataset 3 included 395 participants (231 females, age: 35.4 ± 2.6). Note that some participants in this dataset had missing behavioral ratings in some conditions. Considering the lack of sufficient trials per condition, we discarded data from these participants with missing values, which was the reason why the sample sizes in

the main figures were 369, 358, and 371 for the three intensity conditions respectively. Dataset 4 had 124 participants (61 females, age: 22.2 ± 2.7). Dataset 5 included 92 participants (50 females, age: 21.9 ± 3.2). All participants were healthy and free of pain, neurological, or psychiatric disorders. They all gave written informed consent prior to the experiments. Local ethics committees approved the experimental procedures for the original studies (Datasets 1, 2, and 5: Ethics Committee of the Institute of Psychology at the Chinese Academy of Science; Dataset 3: Institutional Review Board of the University of Colorado Boulder; Dataset 4: Sungkyunkwan University Institutional Review Board).

Sensory stimulation

Three different types of painful stimuli were used in these datasets: (1) laser heat pain: Datasets 1 and 2; (2) mechanical pain: Dataset 3; (3) contact heat pain: Datasets 4 and 5. Datasets 1 and 2 also delivered three kinds of nonpainful stimuli: (1) electro-tactile, (2) auditory, and (3) visual stimuli.

In Datasets 1 and 2, laser heat pain stimuli were transient radiant heat pulses (wavelength: 1.34μm; pulse duration: 4ms) generated by an infrared neodymium yttrium aluminum perovskite (Nd: YAP) laser (Electronical Engineering, Italy). The laser beam was transmitted by an optic fiber, and its diameter was set at approximately 7mm. Laser pulses were delivered to a pre-defined square ($5\times5cm^2$) on the left-hand dorsum. After each stimulus, the laser beam was displaced by approximately 1cm in a random direction to avoid nociceptor fatigue or sensitization. Two stimulus energies (3.0J and 3.5J) were used in Dataset 1, and two other stimulus energies (3.5J and 4.0J) were used in Dataset 2. A stimulus intensity of 3.0J was adopted in Dataset 1 because nociceptive laser stimuli of 4.0J were unbearable for these participants. In Dataset 3, mechanical pain stimuli were delivered to the fingers of the left hand for 10s with an MRI-compatible pressure pain device. There were three levels of physical intensity, 6 kg/cm^2, 7 kg/cm^2, and 8kg/cm^2. In Datasets 4, contact heat pain stimuli were administered to the volar surface of the left forearm with a $16\times16mm^2$ ATS thermode of a Pathway system (Medoc Ltd, Ramat Yishai, Israel). The target temperature of the stimuli was 47.5°C with the baseline temperature being 32°C. The stimulation lasted for 12s (ramp-up: 2.5s; plateau: 7s; ramp-down: 2.5s).

In Dataset 5, contact heat pain stimuli were delivered to the C5~C6 dermatomes on both forearms with a 573mm^2 (diameter of 27mm) CHEPS thermode using a Pathway system (Medoc Ltd, Ramat Yishai, Israel). The heat stimulation ramped up from a baseline of 32°C to a temperature for 3s that led to a perceived intensity rating of 7 on a 0~10 rating scale. In other words, the target temperature was tailored individually for each participant to ensure a constant perceived intensity.

In Datasets 1 and 2, nonpainful stimuli were also delivered. Non-nociceptive tactile stimuli were constant current square-wave electrical pulses (duration: 1ms; model DS7A, Digitimer, UK) delivered through a pair of skin electrodes (1cm interelectrode distance) placed on the left wrist, over the superficial radial nerve. The same two stimulus intensities (2.0mA and 4.0mA) were used in both datasets. Auditory stimuli were brief pure tones (frequency: 800Hz; duration: 50ms; 5ms rise and fall time) delivered through a headphone. The same two stimulus intensities (76dB SPL and 88dB SPL) were used for all participants in both datasets. Visual stimuli were brief flashes of a grey round disk in a black background (duration: 100ms) on a computer screen. The stimulus intensities were adjusted using the greyscale of the round disk, corresponding to RGB values of (100, 100, 100) and (200, 200, 200), respectively, for all participants in both datasets. Stimulus intensities of tactile, auditory, and visual stimuli were determined based on a pilot behavioral experiment to ensure that the perceived ratings of low and high intensity stimuli were approximately 4 and 7 out of 10, respectively.

Study design

The original authors reported their study designs in great detail[14,17,40,41]. Since these papers were all openly accessible, here we only briefly described the study design of each dataset (Figure 1B).

In Datasets 1 and 2, participants received 80 transient stimuli of four different sensory modalities (nociceptive laser, non-nociceptive tactile, auditory, and visual) divided into two runs, and then rated their perceived intensity with a rating scale ranging from 0 (‘‘no sensation’’) to 10 (‘‘the strongest sensation imaginable [in each stimulus modality]’’). For

each sensory modality, two stimulus intensities (i.e., high and low) were delivered. In other words, each participant underwent eight experimental conditions (4 modalities×2 intensities), each condition with 10 trials. The only difference in the study design of Datasets 1 and 2 was the physical intensity of laser heat pain stimuli (detailed in **Sensory stimulation**).

Dataset 3 adopted a within-subjects design to examine the neural mechanisms of placebo analgesia. The study consisted of a verbal suggestion phase, a conditioning phase, and a test phase. Verbal suggestions and conditioning were used to induce placebo effects. In the verbal suggestion phase, two identical creams were introduced to participants, one being a placebo cream that was claimed to have a pain-relieving effect, the other being a control cream claimed to have no analgesic effects. These two creams were applied to two different fingers of the left hand. Then participants went through the conditioning phase, where they experienced the analgesic effect of the placebo cream through social observational learning and classical conditioning. Importantly, in this conditioning phase, only contact heat pain stimuli were delivered. Finally, in the test phase, participants received both contact heat pain and mechanical pain stimuli in the fingers with the placebo and control creams. The test phase delivered a total of 32 stimuli in four runs, with four thermal and four mechanical stimuli in a random order per run. After each stimulus, participants rated the intensity of the stimulus with a 0~1 rating scale, where 0 means “no pain”, 0.014 “barely detectable”, 0.061 “weak pain”, 0.172 “moderate pain”, 0.354 “strong pain”, and 1 “most intense sensation imaginable”.

In Dataset 4, participants received contact heat pain stimuli of six intensity levels in their left forearm. The entire study consisted of eight pain task runs with 12 trials each run and 16 trials per temperature. After each stimulus, participants rated the perceived intensity of the stimuli with a 0~1 rating scale (0, “no sensation”; 0.061, “weak”; 0.172, “moderate”; 0.3454, “strong”; 0.533, “very strong”; 1, “strongest imaginable”). Note that the original authors only shared data for the highest temperature condition (i.e., 47.5°C). We thus could only analyze data for this condition.

Different from Datasets 1~4, Dataset 5 adopted a between-subjects design to investigate the cortico-spinal mechanisms of TENS-induced analgesia. Participants were randomly assigned to three groups: conventional TENS (c-TENS), acupuncture-like TENS (a-TENS), and sham TENS. Each participant experienced 60 contact heat pain stimuli (pre-treatment session: 15 stimuli in the left arm and 15 stimuli in the right arm; post-treatment session: 15 stimuli in the left arm and 15 stimuli in the right arm) in two runs and then reported their perceived intensity and unpleasantness in a 0~10 ratings scale (0: "no feeling/unpleasantness"; 10: "unbearable pain/extreme unpleasantness"). Note that we only used data from the 15 stimuli delivered to the left arm, since painful stimuli were only delivered to the left hand in other datasets. We pooled data from all three groups. The purpose was twofold. First, we could have a large sample size and thus a larger statistical power. Second, our goal was to test whether NIPS could predict the amount of pain reduction after the treatment compared with the pre-treatment baseline, not the analgesic effect of verum TENS compared with sham TENS. Indeed, pain sensitivity could also change after the sham TENS treatment due to factors like natural history, regression to the mean, and so on. A model that predicts pain reduction should thus also predict sensitivity change in the sham TENS condition.

MRI acquisition

Details of the MRI acquisition parameters can be found in Table S2&S3.

Image preprocessing

We analyzed preprocessed data from the original studies[14,17,40,41]. Detailed preprocessing descriptions can be found in these papers. For Datasets 1&2, fMRI data were preprocessed using Statistical Parametric Mapping 12 (SPM12) (Wellcome Trust Center for Neuroimaging, London). The preprocessing included: (1) removing the first three volumes in each run; (2) slice-time correction using the second slice and realignment to the mean slice; (3) co-registration; (4) normalizing to the Montreal Neurological Institute (MNI) space (resampling voxel size = $3\times3\times3mm^3$); (5) regressing out five principal components of the white matter (WM) and cerebrospinal fluid (CSF) signals, and the six motion

parameters; (6) smoothing with a 6mm full-width at half maximum (FWHM) Gaussian kernel.

For Dataset 3, images were preprocessed with fMRIprep ver. 20.2.3[68]. Briefly, the preprocessing included: (1) motion-correction with MCFLIRT (FSL 5.0.9); (2) co-registering to the T1 reference using the boundary-based registration method (BBR) (FreeSurfer); (3) normalizing to the standard space; (4) smoothing with a 6mm FWHM Gaussian kernel.

For Dataset 4, preprocessing was performed with SPM12 and FSL, including (1) removing the first 18 volumes for each run; (2) realignment; (3) co-registration; (4) normalizing to the MNI space (2×2×2 mm^3); (5) smoothing with a 5mm FWHM Gaussian kernel; (6) reducing motion-related artifacts with the Independent Component Analysis-based strategy for Automatic Removal Of Motion Artifacts; (7) removing data where the mean frame displacement (FD) of a run > 0.2mm, or the FD of any volume > 5mm.

For Dataset 5, preprocessing was also conducted using FSL, with the following steps: (1) physiological noise (i.e., respiratory and cardiac noise) regression with the physiological noise model toolbox; (2) distortion correction with the TOPUP tool; (3) slice timing correction with the *slicetimer* function; (4) motion-correction with MCFLIRT; (5) brain extraction with the BET; (6) smoothing with a 5mm FWHM Gaussian kernel; (7) high-pass filtering (cutoff: 100s); (8) co-registration with the BBR; (9) normalizing to the MNI space (2×2×2 mm^3) with FNIRT.

fMRI data analysis

First level analysis

We mainly reanalyzed first level contrast images from the original studies[14,17,40,41]. In Datasets 1&2, regressors in the first level analysis included eight conditions (4 modalities×2 intensities) convolved with the canonical hemodynamic response function, its temporal derivatives, and six head motion estimates. Moreover, we high-pass filtered images with a cutoff period of 128s and accounted for temporal autocorrelations using the

first-order autoregressive model (AR(1)). In Dataset 3, regressors in the first level analysis included all experimental conditions convolved with the canonical hemodynamic response function, 24 motion parameters, and mean CSF signal. A high-pass filter of 180s was also applied. In Dataset 4, a single trial approach was utilized. Regressors included every single pain trial convolved with the canonical hemodynamic response function, five principal components of WM and CSF signal, and a linear trend. Signals were also filtered with an 180s high-pass filter. Trials with a variance inflation factor > 3 were subsequently removed. Single trial beta maps were finally averaged to derive the beta map for painful stimulation. In Dataset 5, regressors included painful stimulation and rating period convolved with the canonical hemodynamic response function and its temporal derivatives.

Second level correlational analysis

To examine the relationship between pain-evoked BOLD responses and pain sensitivity, we correlated first level beta maps in each pain condition with average pain ratings. The significance threshold was set at p(FDR) = 0.05 (two-tailed). To test the robustness of results, we computed both Pearson's r and Spearman's rho in the correlational analyses. In addition to whole brain analysis, we also conducted an ROI analysis. Specifically, we extracted mean signals from classical pain-related areas[15,16], namely, the S1, S2, ACC, insula, and thalamus using anatomically defined masks defined with the Harvard-Oxford Atlas distributed with FSL[69]. Note that the Harvard-Oxford Atlas is a probabilistic atlas and we thresholded probability maps for each region at 50%[70].

To test the pain selectivity of the correlation between BOLD responses and sensory sensitivity, we also performed the same correlational analysis for touch, audition, and vision in Datasets 1&2. To directly test the significance of correlation differences, we compared the correlation coefficients between modalities[45]. The statistic for this comparison is defined as

$$z = \frac{z_1 - z_2}{\sqrt{\frac{1}{n_1 - 3} + \frac{1}{n_2 - 3}}}$$

where z_1 and z_2 are the Fisher Z-transformed correlation coefficients, and n_1 and n_2 are the sample sizes.

Note that all statistical tests in the article are two-sided unless stated otherwise.

Sensitivity matching procedure

Although the physical intensity of sensory stimuli was fixed in Datasets 1&2, perceived intensity ratings (i.e., sensory sensitivity) were significantly different among different modalities. Distinct correlational results in pain and nonpain modalities could thus be potentially attributed to intensity rating differences. Furthermore, perceived intensity ratings are highly correlated with stimulus salience[34]. As a result, differences in perceptual ratings may result in incompatible salience levels between modalities. To control for this possible confounding factor of rating differences, we adopted a rating matching procedure to equalize intensity ratings between pain and nonpain modalities. To rule out the influence of individual differences, we matched pain intensity ratings and tactile/auditory/visual intensity ratings in a within-individual manner. Specifically, we manually screened participants whose pain intensity ratings in the 3.5J condition and tactile/auditory/visual intensity ratings in the high intensity condition were not significantly different, namely the 95% confidence interval of the rating differences contained 0. With this matching criterion, 192 participants were selected for the pain-touch comparison, 171 for the pain-audition comparison, and 147 for the pain-vision comparison (Figure 5A~C).

Resampling procedure

We used a resampling method to examine the influence of sample sizes on the probability of detecting significant correlations between BOLD responses and pain sensitivity. In the pooled 3.5J data from Datasets 1&2 (N = 399), we generated bootstrapped subsamples from the whole dataset, that is, randomly selected data samples with replacement. The sample size of these subsamples ranged from 100 to 400 (in steps of 10), and, for each sample size, the resampling procedure was repeated 100 times. In each subsample, we correlated BOLD responses with pain sensitivity and thresholded the correlation maps with p(FDR) = 0.05. Since we generated 100 subsamples for each sample size, the probability of a voxel being significant under a certain sample size can be approximated as the number

of times that voxel reached significance. We then calculated the sample size needed for each voxel to pass the p(FDR) = 0.05 threshold with a probability of 0.8[44].

To supplement this whole brain analysis, we also conducted the resampling in an ROI analysis manner. Specifically, we defined anatomical masks for the S1, S2, ACC, insula, and thalamus using the Harvard-Oxford Atlas[69] distributed with FSL. Note that the probability maps for each region were thresholded at 50%[70]. Subsequently, we generated 1000 bootstrapped subsamples with sample sizes from 10 to 400 (in steps of 10). In this ROI analysis, we set the significance to α = 0.01 or α = 0.001, and then made line charts to fully show the relationship between sample sizes and the probability of significance for each ROI.

To test the robustness of the findings from the foregoing resampling method, we also conducted the whole brain and ROI analyses with data for 8kg/cm^2 condition in Dataset 3 (N = 369). Note that the upper bound of the exampled sample size was set to 370 due to a slightly smaller sample size for Dataset 3.

Machine learning

Model development

We split randomly the pooled 3.5J data in Datasets 1&2 into a Discovery Set (N = 199) and a Holdout Test Set (N = 200). A LASSO-PCR model was trained to predict pain sensitivity using first level t maps in the Discovery Set with Scikit-learn (ver 1.3.0; https://scikit-learn.org/stable/index.html). The LASSO is a regularization method that shrinks the linear regression coefficient estimates toward zero[71]. Mathematically, LASSO regression minimizes the following loss function:

$$Loss = \sum_{i=1}^{n}(y_i - \beta_0 - \sum_{j=1}^{p}\beta_j x_{ij})^2 + \lambda \sum_{j=1}^{p}|\beta_j|$$

where y_i is the predicted variable of participant i, β_0 and β_j are the linear regression coefficient estimates, x_{ij} is the j-th predictor for participant i, λ is the tuning parameter, n is the number of participants, and p is the number of predictors.

T maps were first standardized across participants and then submitted to principal component analysis to reduce the feature dimensions. Principal components were used as features in the LASSO regression model. Five-fold cross-validation was used to evaluate model performance. The predictive performance of the final model was assessed using two metrics: (1) Pearson's correlation coefficient between the predicted and real pain sensitivity, and (2) R^2, a metric representing the proportion of variance explained by the model. R^2 is defined as:

$$R^2 = 1 - \frac{\sum_{i=1}^{n}(y_i - \hat{y}_i)^2}{\sum_{i=1}^{n}(y_i - \bar{y}_i)^2}$$

where y_i is the real value for *i*-th data point, $\hat{y}_i$ is the predicted value, and $\bar{y}_i$ is the mean of all real values. Note that R^2 is not identical to the square of Pearson's correlation, and can be negative if model performance is worse than a simple mean prediction, that is, using $\bar{y}_i$ as predictions for all data points.

To determine the optimal tuning parameter λ, we selected 100 λ values log-uniformly distributed in the $[10^{-2}, 10^{2}]$ interval and tuned λ according to the cross-validated mean squared errors. The optimal λ was 0.236.

Model testing

After our model (i.e., NIPS) was developed, we tested its performance in the Holdout Test Set. To compare NIPS and other well-recognized models, we applied the Neurological Pain Signature (NPS)[36] and Stimulus Intensity Independent Pain Signature-1 (SIIPS1)[37] to the Holdout Test Set. We also built a simple model based on the pain-related activation pattern derived from a term-based meta-analysis with neurosynth (Neurosynth "pain" model)[72]. The predicted values (model expression) of these three models were the dot product of the weight maps of the models and the first level t map. Pearson's correlation coefficients between predicted and real values were also directly compared to test if NIPS performed better than these three models.

NIPS was developed with laser heat pain data in Datasets 1&2. To test its generalizability, we then applied the model to mechanical pain data in Dataset 3 and contact heat pain data

in Dataset 4. Note that the original authors of Datasets 3&4 shared beta maps for pain, not t maps. NIPS's performance in these two datasets may thus be slightly affected due to scaling issues in beta maps.

To examine the influence of sample size on NIPS's performance, we refitted the model with different training sample sizes with the "*learning_curve*" function in Scikit-learn. The *learning_curve* function generates a curve showing how the performance of the model changes as the training sample size grows. We first randomly shuffled the pooled 3.5J data in Datasets 1&2, and then inputted the model and the shuffled dataset to the *learning_curve* function. We considered training sample sizes from 20 to 300 (in steps of 5). This whole process was repeated 100 times to also estimate the variability of the relationship between training sample size and model performance.

Model interpretation

We employed two approaches to interpret NIPS's weight maps: virtual lesion[47] and neurotransmitter receptor profiling with neuromaps[48]. For virtual lesion, we parcellated NIPS's weight map according to the Automatic Anatomical Labeling template[49] and removed areas one by one or kept areas one by one to examine each area's contribution to the model performance. To reveal the neurotransmitter receptor profile of NIPS, we then correlated its weight map with the spatial distribution maps of major neurotransmitter receptors with the neuromaps toolbox (ver. 0.0.4)[48]. The neurotransmitter receptors we examined included: (1) alpha-4 beta-2 nicotinic receptor (a4b2)[73]; (2) muscarinic acetylcholine receptor subtype M1[74]; (3) vesicular acetylcholine transporter (VAChT)[75]; (4) cannabinoid type-1 receptor (CB1)[76]; (5) dopamine D1-type receptor[77]; (6) dopamine D2-type receptor[78]; (7) respective dopamine transporter (DAT)[79]; (8) GABAa receptor[80]; (9) metabotropic glutamate type 5 receptor (mGluR5)[81]; (10) histamine H3 receptors[82]; (11) μ-opioid receptor (MOR)[83]; (12) norepinephrine transporter (NET)[84]; (13) serotonin 1A receptor (5-HT1a)[85]; (14) 5-HT1b[86]; (15) 5-HT2a[86]; (16) 5-HT4[86]; (17) 5-HT6[87]; (18) serotonin transporter (5-HTT)[86]. To determine the statistical significance, we used the spin test with 10000 permutations[88]. Since the weight map of NIPS was correlated with MOR, NIPS could be associated with pain modulation. To empirically test this hypothesis and

assess NIPS's transferability, we applied NIPS to Datasets 3&5 to predict their analgesic effects from different pain treatments.

Data and code availability

The data and code for all results will be made available on the Open Science Framework (OSF) upon publication. Source data and code for the development and test of NIPS are available on OSF (https://osf.io/y2n34/). Run each cell in "NIPS development and test.ipynb" to reproduce how NIPS was developed and tested.

Acknowledgment

We thank Yu-Xin Chen, Xin Hou, Xiao-Yun Li, Guang-Yue Tian, Wen-Xin Su, Fei-Xue Wang, Jia-Hui Zhong, and Yu-Pu Zhu for their assistance in data collection. We also thank colleagues collecting Datasets 3&4 for kindly sharing their data. This work was supported by the National Key Research and Development Program of China (2023YFC2508702), National Natural Science Foundation of China (32071061), and Beijing Natural Science Foundation (JQ22018).

Author Contributions

Conceptualization: LBZ, LH; Methodology: LBZ, LH; Investigation: HJZ, LH, ZXW, LBZ; Formal analysis: LBZ, LH; Visualization: LBZ, LH; Writing – original draft: LBZ; Writing – review & editing: LBZ, XJL, HJZ, ZXW, YZK, YHT, GDI, LH; Funding acquisition: LH; Project administration: LH; Supervision: LH.

Competing interests

The authors declare no competing interests.

References

1. Mogil, J. S. Sources of individual differences in pain. *Annual Review of Neuroscience* **44**, 1–25 (2021).
2. Campbell, P., Foster, N. E., Thomas, E. & Dunn, K. M. Prognostic Indicators of Low Back Pain in Primary Care: Five-Year Prospective Study. *The Journal of Pain* **14**, 873–883 (2013).
3. Nielsen, C. S., Staud, R. & Price, D. D. Individual differences in pain sensitivity: measurement, causation, and consequences. *The Journal of Pain* **10**, 231–237 (2009).
4. Werner, M. U., Mjöbo, H. N., Nielsen, P. R., Rudin, Å. & Warner, D. S. Prediction of Postoperative Pain: A Systematic Review of Predictive Experimental Pain Studies. *Anesthesiology* **112**, 1494–1502 (2010).
5. Fayaz, A., Croft, P., Langford, R. M., Donaldson, L. J. & Jones, G. T. Prevalence of chronic pain in the UK: a systematic review and meta-analysis of population studies. *BMJ Open* **6**, e010364 (2016).
6. Johannes, C. B., Le, T. K., Zhou, X., Johnston, J. A. & Dworkin, R. H. The prevalence of chronic pain in United States adults: results of an internet-based survey. *The Journal of Pain* **11**, 1230–1239 (2010).
7. Davis, K. D. *et al.* Discovery and validation of biomarkers to aid the development of safe and effective pain therapeutics: challenges and opportunities. *Nature Reviews Neurology* **16**, 381–400 (2020).
8. Tracey, I. Neuroimaging enters the pain biomarker arena. *Science Translational Medicine* **13**, eabj7358 (2021).
9. Woolf, C. J. & Max, M. B. Mechanism-based Pain Diagnosis: Issues for Analgesic Drug Development. *Anesthesiology* **95**, 241–249 (2001).
10. Coghill, R. C., McHaffie, J. G. & Yen, Y.-F. Neural correlates of interindividual differences in the subjective experience of pain. *Proceedings of the National Academy of Sciences* **100**, 8538–8542 (2003).
11. Hoeppli, M. E. *et al.* Dissociation between individual differences in self-reported pain intensity and underlying fMRI brain activation. *Nature Communications* **13**, 3569 (2022).
12. Spisak, T. *et al.* Pain-free resting-state functional brain connectivity predicts individual pain sensitivity. *Nature Communications* **11**, 187 (2020).
13. Tu, Y. *et al.* Identifying inter-individual differences in pain threshold using brain connectome: a test-retest reproducible study. *NeuroImage* **202**, 116049 (2019).
14. Zhang, L.-B. *et al.* Selective and replicable neuroimaging-based indicators of pain discriminability. *Cell Reports Medicine* **3**, 100846 (2022).
15. Apkarian, A. V., Bushnell, M. C., Treede, R.-D. & Zubieta, J.-K. Human brain mechanisms of pain perception and regulation in health and disease. *European Journal of Pain* **9**, 463–463 (2005).
16. Xu, A. *et al.* Convergent neural representations of experimentally-induced acute pain in healthy volunteers: A large-scale fMRI meta-analysis. *Neuroscience & Biobehavioral Reviews* **112**, 300–323 (2020).
17. Gim, S., Lee, D. H., Lee, S. & Woo, C.-W. Interindividual differences in pain can be explained by fMRI, sociodemographic, and psychological factors. 2023.07.06.547919 Preprint at https://doi.org/10.1101/2023.07.06.547919 (2023).
18. Baker, M. 1,500 scientists lift the lid on reproducibility. *Nature* **533**, 452–454 (2016).

19. Button, K. S. *et al.* Power failure: why small sample size undermines the reliability of neuroscience. *Nature Reviews Neuroscience* **14**, 365–376 (2013).
20. Open Science Collaboration. Estimating the reproducibility of psychological science. *Science* **349**, aac4716–aac4716 (2015).
21. Poldrack, R. A. *et al.* Scanning the horizon: towards transparent and reproducible neuroimaging research. *Nature Reviews Neuroscience* **18**, 115–126 (2017).
22. Bossier, H. *et al.* The empirical replicability of task-based fMRI as a function of sample size. *NeuroImage* **212**, 116601 (2020).
23. Liu, S., Abdellaoui, A., Verweij, K. J. H. & van Wingen, G. A. Replicable brain–phenotype associations require large-scale neuroimaging data. *Nature Human Behaviour* 1–13 (2023) doi:10.1038/s41562-023-01642-5.
24. Marek, S. *et al.* Reproducible brain-wide association studies require thousands of individuals. *Nature* **603**, 654–660 (2022).
25. Schönbrodt, F. D. & Perugini, M. At what sample size do correlations stabilize? *Journal of Research in Personality* **47**, 609–612 (2013).
26. Mouraux, A. & Iannetti, G. D. The search for pain biomarkers in the human brain. *Brain* **141**, 3290–3307 (2018).
27. Hu, L. & Iannetti, G. D. Neural indicators of perceptual variability of pain across species. *Proceedings of the National Academy of Sciences* **116**, 1782–1791 (2019).
28. Mouraux, A., Diukova, A., Lee, M. C., Wise, R. G. & Iannetti, G. D. A multisensory investigation of the functional significance of the 'pain matrix'. *NeuroImage* **54**, 2237–2249 (2011).
29. Ronga, I., Valentini, E., Mouraux, A. & Iannetti, G. D. Novelty is not enough: laser-evoked potentials are determined by stimulus saliency, not absolute novelty. *Journal of Neurophysiology* **109**, 692–701 (2012).
30. Su, Q. *et al.* Brain regions preferentially responding to transient and iso-intense painful or tactile stimuli. *NeuroImage* **192**, 52–65 (2019).
31. Horing, B., Sprenger, C. & Büchel, C. The parietal operculum preferentially encodes heat pain and not salience. *PLOS Biology* **17**, e3000205 (2019).
32. Zhang, X. *et al.* A multisensory fMRI investigation of nociceptive-preferential cortical regions and responses. *Frontiers in Neuroscience* **15**, (2021).
33. Tu, Y. *et al.* Pain-preferential thalamocortical neural dynamics across species. *Nature Human Behaviour* **8**, 1–15 (2023).
34. Liang, M., Su, Q., Mouraux, A. & Iannetti, G. D. Spatial patterns of brain activity preferentially reflecting transient pain and stimulus intensity. *Cereb Cortex* **29**, 2211–2227 (2019).
35. Su, Q., Song, Y., Zhao, R. & Liang, M. A review on the ongoing quest for a pain signature in the human brain. *Brain Science Advances* **5**, 274–287 (2020).
36. Wager, T. D. *et al.* An fMRI-based neurologic signature of physical pain. *New England Journal of Medicine* **368**, 1388–1397 (2013).
37. Woo, C.-W. *et al.* Quantifying cerebral contributions to pain beyond nociception. *Nature Communications* **8**, 1–14 (2017).
38. Grouper, H., Eisenberg, E. & Pud, D. The relationship between sensitivity to pain and conditioned pain modulation in healthy people. *Neuroscience Letters* **708**, 134333 (2019).

39. Skovbjerg, S. *et al.* Conditioned Pain Modulation and Pressure Pain Sensitivity in the Adult Danish General Population: The DanFunD Study. *The Journal of Pain* **18**, 274–284 (2017).
40. Botvinik-Nezer, R. *et al.* Placebo treatment affects brain systems related to affective and cognitive processes, but not nociceptive pain. 2023.09.21.558825 Preprint at https://doi.org/10.1101/2023.09.21.558825 (2023).
41. Wei, Z. *et al.* Cortico-spinal Mechanisms of Periphery Neuromodulation induced Analgesia. 2024.02.06.579059 Preprint at https://doi.org/10.1101/2024.02.06.579059 (2024).
42. Wen, Z. *et al.* Temporally and anatomically specific contributions of the human amygdala to threat and safety learning. *Proceedings of the National Academy of Sciences* **119**, e2204066119 (2022).
43. Friston, K. J., Williams, S., Howard, R., Frackowiak, R. S. J. & Turner, R. Movement-Related effects in fMRI time-series. *Magnetic Resonance in Medicine* **35**, 346–355 (1996).
44. Cohen, J. *Statistical Power Analysis for the Behavioral Sciences*. (Lawrence Erlbaum Associates, Hillsdale, NJ, 1988).
45. Steiger, J. H. Tests for comparing elements of a correlation matrix. *Psychological Bulletin* **87**, 245–251 (1980).
46. Henson, R. What can functional neuroimaging tell the experimental psychologist? *The Quarterly Journal of Experimental Psychology Section A* **58**, 193–233 (2005).
47. Kohoutová, L. *et al.* Toward a unified framework for interpreting machine-learning models in neuroimaging. *Nature Protocols* **15**, 1399–1435 (2020).
48. Markello, R. D. *et al.* neuromaps: structural and functional interpretation of brain maps. *Nature Methods* **19**, 1472–1479 (2022).
49. Tzourio-Mazoyer, N. *et al.* Automated Anatomical Labeling of Activations in SPM Using a Macroscopic Anatomical Parcellation of the MNI MRI Single-Subject Brain. *NeuroImage* **15**, 273–289 (2002).
50. Coghill, R. C. The distributed nociceptive system: a framework for understanding pain. *Trends in Neurosciences* **43**, 780–794 (2020).
51. Zubieta, J.-K. *et al.* Regional Mu Opioid Receptor Regulation of Sensory and Affective Dimensions of Pain. *Science* **293**, 311–315 (2001).
52. Melum, T. A. *et al.* Gray matter volume and pain tolerance in a general population: the Tromsø study. *PAIN* **164**, 1750 (2023).
53. Schulz, E., Zherdin, A., Tiemann, L., Plant, C. & Ploner, M. Decoding an individual's sensitivity to pain from the multivariate analysis of EEG data. *Cerebral Cortex* **22**, 1118–1123 (2012).
54. Kotikalapudi, R. *et al.* Brain morphology predicts individual sensitivity to pain: a multicenter machine learning approach. *PAIN* **164**, 2516 (2023).
55. Finn, E. S. Is it time to put rest to rest? *Trends in Cognitive Sciences* **25**, 1021–1032 (2021).
56. Greene, A. S., Gao, S., Scheinost, D. & Constable, R. T. Task-induced brain state manipulation improves prediction of individual traits. *Nature Communications* **9**, 2807 (2018).
57. Kim, H. J. *et al.* Racial and ethnic differences in experimental pain sensitivity: systematic review and meta-analysis. *PAIN* **158**, 194 (2017).

58. Losin, E. A. R. *et al.* Neural and sociocultural mediators of ethnic differences in pain. *Nature Human Behaviour* 1–14 (2020) doi:10.1038/s41562-020-0819-8.
59. Goltermann, O. & Büchel, C. Improving fMRI-based prediction of individual pain ratings by accounting for interindividual variance. 2023.07.06.548050 Preprint at https://doi.org/10.1101/2023.07.06.548050 (2023).
60. Szucs, D. & Ioannidis, J. PA. Sample size evolution in neuroimaging research: An evaluation of highly-cited studies (1990–2012) and of latest practices (2017–2018) in high-impact journals. *NeuroImage* **221**, 117164 (2020).
61. Yeung, A. W. K. An Updated Survey on Statistical Thresholding and Sample Size of fMRI Studies. *Frontiers in Human Neuroscience* **12**, (2018).
62. Cui, Z. & Gong, G. The effect of machine learning regression algorithms and sample size on individualized behavioral prediction with functional connectivity features. *NeuroImage* **178**, 622–637 (2018).
63. Lee, D. H., Lee, S. & Woo, C.-W. Decoding Pain: Uncovering the Factors that Affect Performance of Neuroimaging-Based Pain Models. 2023.12.22.573021 Preprint at https://doi.org/10.1101/2023.12.22.573021 (2023).
64. Schulz, M.-A., Bzdok, D., Haufe, S., Haynes, J.-D. & Ritter, K. Performance reserves in brain-imaging-based phenotype prediction. *Cell Reports* **43**, 113597 (2024).
65. Spisak, T., Bingel, U. & Wager, T. D. Multivariate BWAS can be replicable with moderate sample sizes. *Nature* **615**, E4–E7 (2023).
66. Turner, B. O., Paul, E. J., Miller, M. B. & Barbey, A. K. Small sample sizes reduce the replicability of task-based fMRI studies. *Communications Biology* **1**, 1–10 (2018).
67. Schulz, M.-A. *et al.* Different scaling of linear models and deep learning in UKBiobank brain images versus machine-learning datasets. *Nature Communications* **11**, 4238 (2020).
68. Esteban, O. *et al.* fMRIPrep: a robust preprocessing pipeline for functional MRI. *Nature Methods* **16**, 111–116 (2019).
69. Desikan, R. S. *et al.* An automated labeling system for subdividing the human cerebral cortex on MRI scans into gyral based regions of interest. *NeuroImage* **31**, 968–980 (2006).
70. Geuter, S., Boll, S., Eippert, F. & Büchel, C. Functional dissociation of stimulus intensity encoding and predictive coding of pain in the insula. *eLife* **6**, (2017).
71. Tibshirani, R. Regression Shrinkage and Selection Via the Lasso. *Journal of the Royal Statistical Society: Series B (Methodological)* **58**, 267–288 (1996).
72. Yarkoni, T., Poldrack, R. A., Nichols, T. E., Van Essen, D. C. & Wager, T. D. Large-scale automated synthesis of human functional neuroimaging data. *Nature Methods* **8**, 665–670 (2011).
73. Hillmer, A. T. *et al.* Imaging of cerebral α4β2* nicotinic acetylcholine receptors with (−)-[18F]Flubatine PET: Implementation of bolus plus constant infusion and sensitivity to acetylcholine in human brain. *NeuroImage* **141**, 71–80 (2016).
74. Naganawa, M. *et al.* First-in-Human Assessment of 11C-LSN3172176, an M1 Muscarinic Acetylcholine Receptor PET Radiotracer. *Journal of Nuclear Medicine* **62**, 553–560 (2021).
75. Aghourian, M. *et al.* Quantification of brain cholinergic denervation in Alzheimer's disease using PET imaging with [18F]-FEOBV. *Molecular Psychiatry* **22**, 1531–1538 (2017).

76. Normandin, M. D. *et al.* Imaging the Cannabinoid CB1 Receptor in Humans with [^{11}C] OMAR: Assessment of Kinetic Analysis Methods, Test–Retest Reproducibility, and Gender Differences. *Journal of Cerebral Blood Flow & Metabolism* **35**, 1313–1322 (2015).
77. Kaller, S. *et al.* Test–retest measurements of dopamine D1-type receptors using simultaneous PET/MRI imaging. *European Journal of Nuclear Medicine and Molecular Imaging* **44**, 1025–1032 (2017).
78. Sandiego, C. M. *et al.* Reference Region Modeling Approaches for Amphetamine Challenge Studies with [^{11}C]FLB 457 and PET. *Journal of Cerebral Blood Flow & Metabolism* **35**, 623–629 (2015).
79. Dukart, J. *et al.* Cerebral blood flow predicts differential neurotransmitter activity. *Scientific Reports* **8**, 4074 (2018).
80. Nørgaard, M. *et al.* A high-resolution in vivo atlas of the human brain's benzodiazepine binding site of GABAA receptors. *NeuroImage* **232**, 117878 (2021).
81. Smart, K. *et al.* Sex differences in [11C]ABP688 binding: a positron emission tomography study of mGlu5 receptors. *European Journal of Nuclear Medicine and Molecular Imaging* **46**, 1179–1183 (2019).
82. Gallezot, J.-D. *et al.* Determination of receptor occupancy in the presence of mass dose: [^{11}C]GSK189254 PET imaging of histamine H_3 receptor occupancy by PF-03654746. *Journal of Cerebral Blood Flow & Metabolism* **37**, 1095–1107 (2017).
83. Kantonen, T. *et al.* Interindividual variability and lateralization of μ-opioid receptors in the human brain. *NeuroImage* **217**, 116922 (2020).
84. Ding, Y.-S. *et al.* PET imaging of the effects of age and cocaine on the norepinephrine transporter in the human brain using (S,S)-[11C]O-methylreboxetine and HRRT. *Synapse* **64**, 30–38 (2010).
85. Savli, M. *et al.* Normative database of the serotonergic system in healthy subjects using multi-tracer PET. *NeuroImage* **63**, 447–459 (2012).
86. Beliveau, V. *et al.* A High-Resolution In Vivo Atlas of the Human Brain's Serotonin System. *Journal of Neuroscience* **37**, 120–128 (2017).
87. Radhakrishnan, R. *et al.* Age-Related Change in 5-HT6 Receptor Availability in Healthy Male Volunteers Measured with 11C-GSK215083 PET. *Journal of Nuclear Medicine* **59**, 1445–1450 (2018).
88. Alexander-Bloch, A. F. *et al.* On testing for spatial correspondence between maps of human brain structure and function. *NeuroImage* **178**, 540–551 (2018).

Figure legends

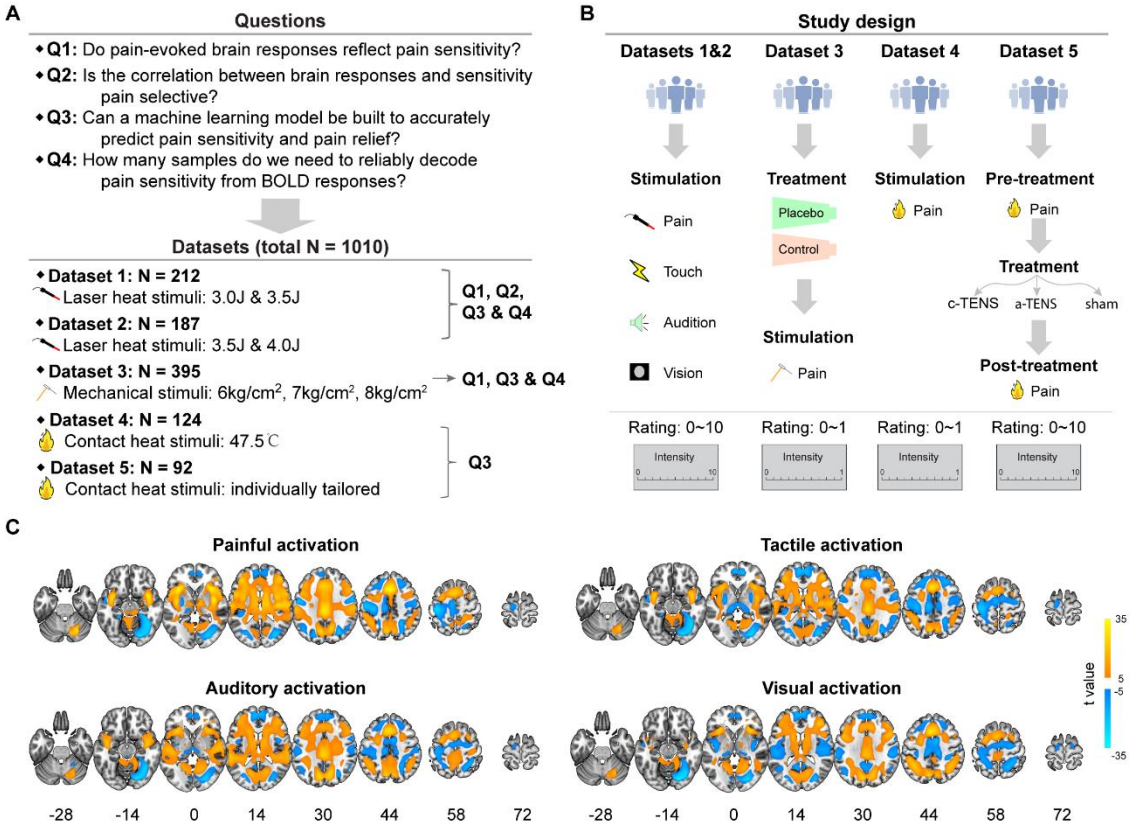

Figure 1. Study overview and brain activations responsive to painful and nonpainful stimuli. (A) Key questions and datasets used to answer these questions. Using five large and diverse datasets with laser heat pain, mechanical pain, and contact heat pain stimuli, we examined the correlation between pain-evoked BOLD responses and pain sensitivity, tested pain selectivity of this correlation, built machine learning models to predict pain sensitivity and pain relief, and explored sample sizes needed to reliably reveal the correlation between BOLD responses and pain sensitivity. **(B)** Study design of five datasets. In all five datasets, participants received sensory stimuli and rated the perceived intensity with a rating scale (from 0 to 10 or from 0 to 1). In Datasets 3&5, participants also received treatments (placebo in Dataset 4 and transcutaneous electrical nerve stimulation [TENS]) to relieve pain. **(C)** Brain areas activated by painful and nonpainful stimuli in Datasets 1&2. Painful, tactile, auditory, and visual stimuli activated largely overlapped brain areas. c-TENS: conventional TENS; a-TENS: acupuncture-like TENS.

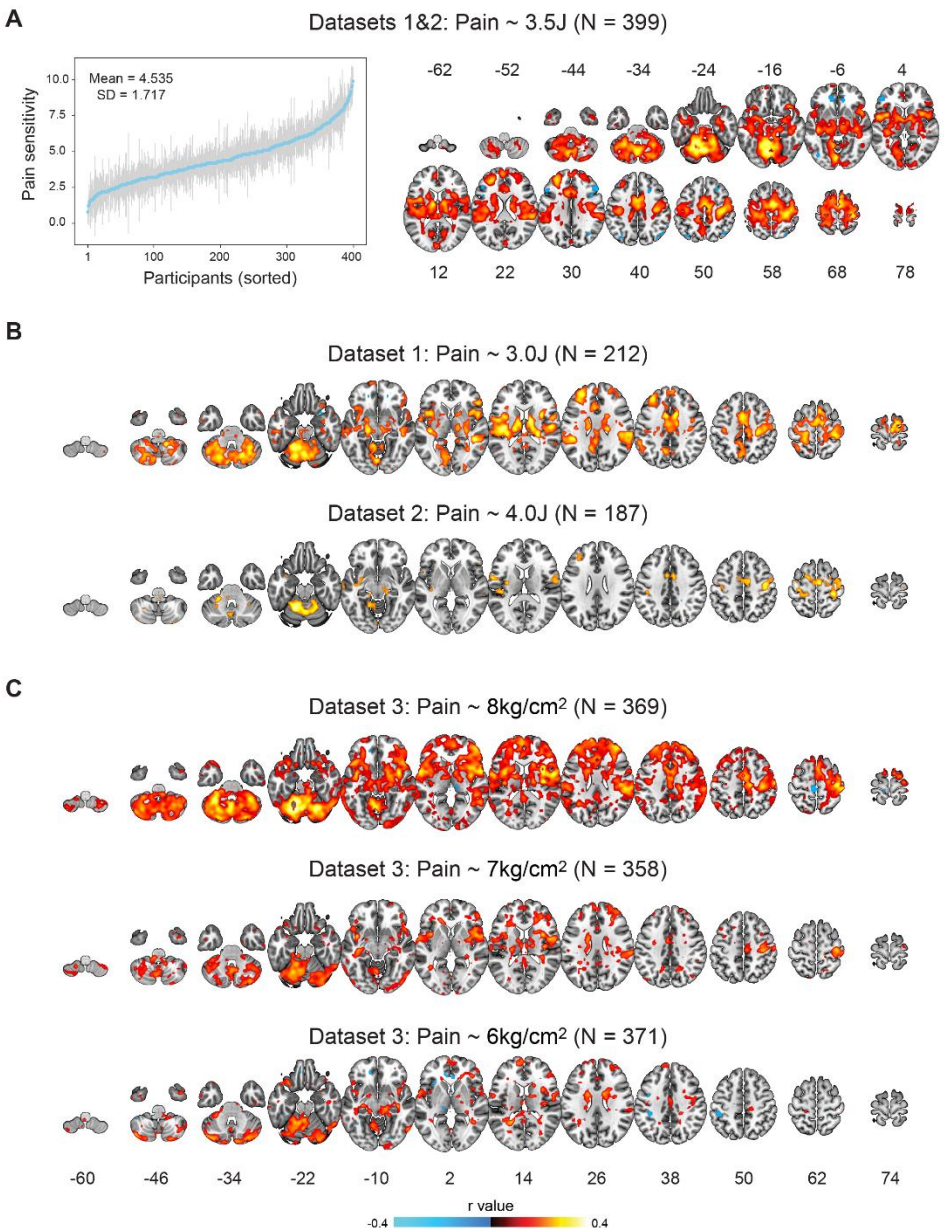

Figure 2. Correlations between pain-evoked BOLD responses and pain sensitivity. (A) BOLD-pain sensitivity correlations in the 3.5J condition in Datasets 1&2. Pain sensitivity varied considerably across individuals. This interindividual variability correlated with pain-evoked BOLD responses in a wide range of areas. **(B)** Replication of the correlation in other conditions in Datasets 1&2. BOLD responses reliably correlated with pain sensitivity in the 3.0J and 4.0J conditions. **(C)** Replication of the correlation in Dataset 3. BOLD responses correlated with mechanical pain sensitivity in all conditions,

demonstrating the replicability and generalizability of the correlation. Error bars in (A) stand for standard deviation (SD) of intensity ratings for each participant.

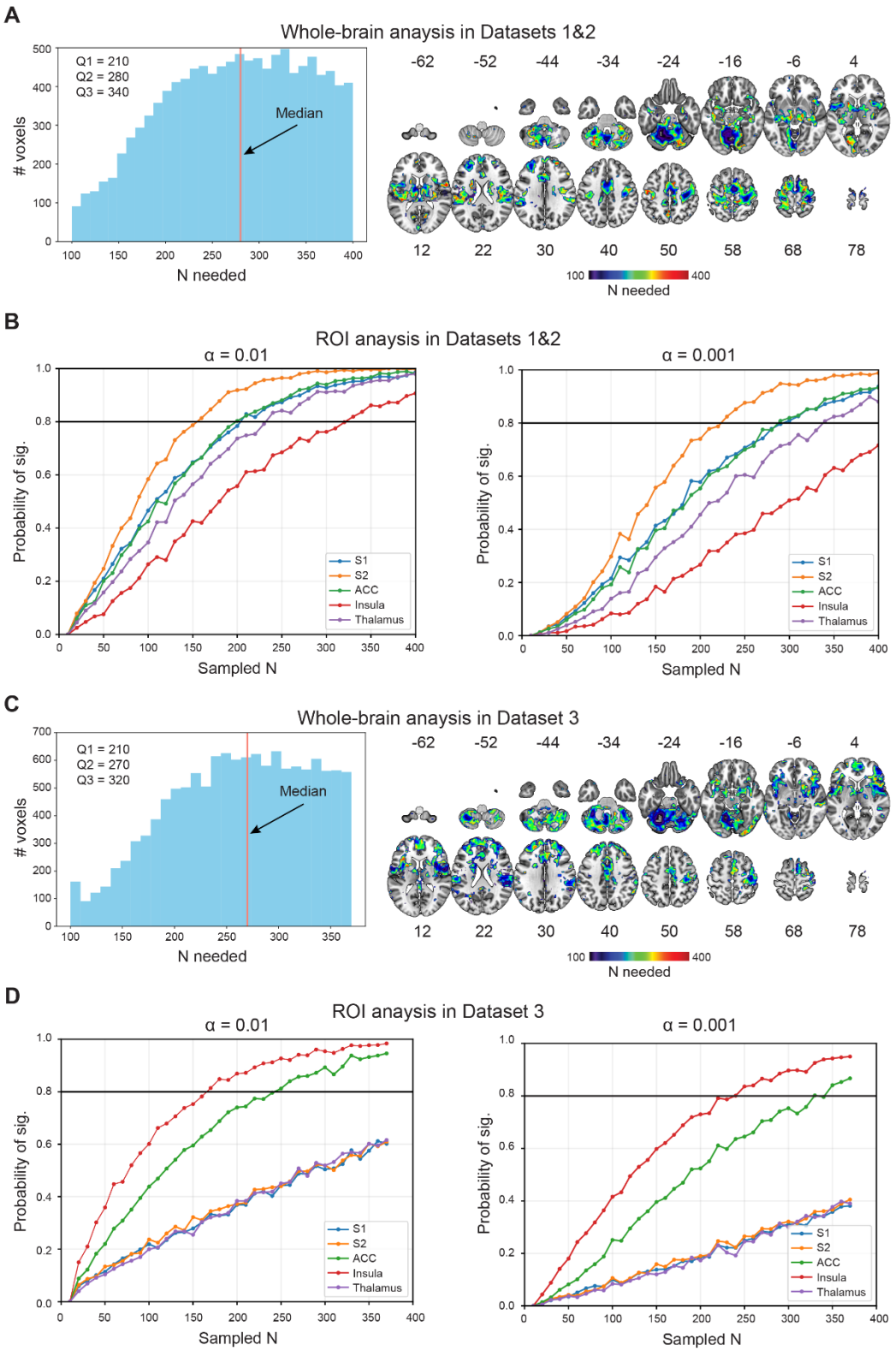

Figure 3. Influence of sample sizes on the detectability of the BOLD responses-pain sensitivity correlation. (A) Sample sizes needed to detect correlation with a probability ≥

0.8 in whole brain analysis in Datasets 1&2. Different sample sizes were needed to reliably detect the correlations in different voxels, and a sample size of 280 was needed to detect half of the correlations. **(B)** Sample sizes needed to detect correlation in ROI analysis in Datasets 1&2. In ROI analysis, large sample sizes were still needed to reliably detect significant correlations. **(C)** Sample sizes needed to detect correlation with a probability ≥ 0.8 in whole brain analysis in Dataset 3. A sample size of 270 was needed to detect half of the correlations. **(D)** Sample sizes needed to detect correlation in ROI analysis in Dataset 3. Q1: first quartile; Q2: second quartile; Q3: third quartile.

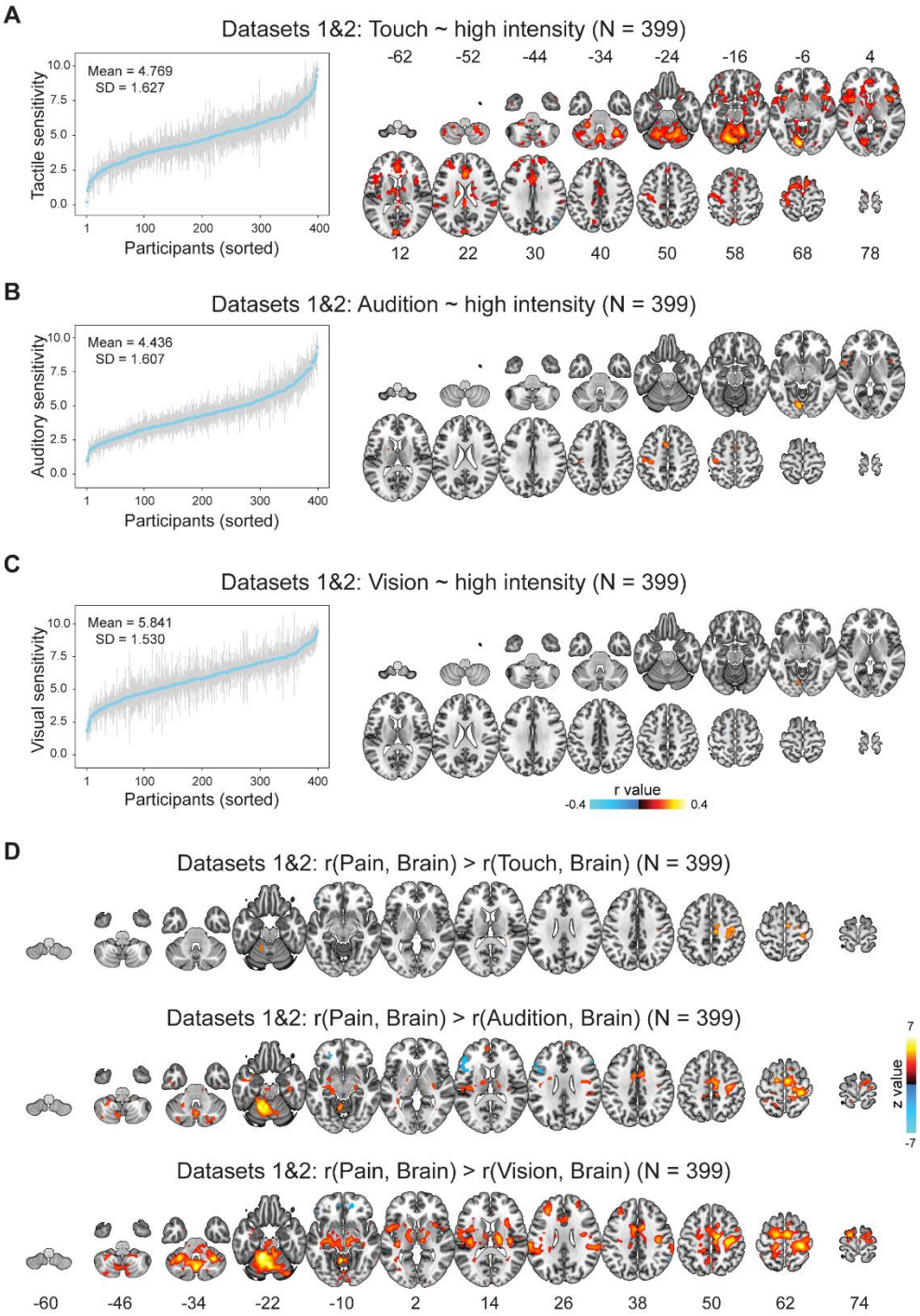

Figure 4. Correlations between BOLD responses and sensory sensitivity in nonpain modalities. (A)~(C) BOLD responses-sensory sensitivity correlation in the high intensity condition in Datasets 1&2 for touch (A), audition (B), and vision (C). Inter-individual variability of tactile sensitivity correlated with BOLD responses in many areas, while only a few areas showed correlation with auditory and visual sensitivity. **(D)** Comparisons of

BOLD-sensitivity correlation between pain and nonpain modalities. Direct comparisons of correlation coefficients showed larger correlations for pain than for touch, audition, and vision. Error bars in (A)~(C) stand for standard deviation (SD) of intensity ratings for each participant.

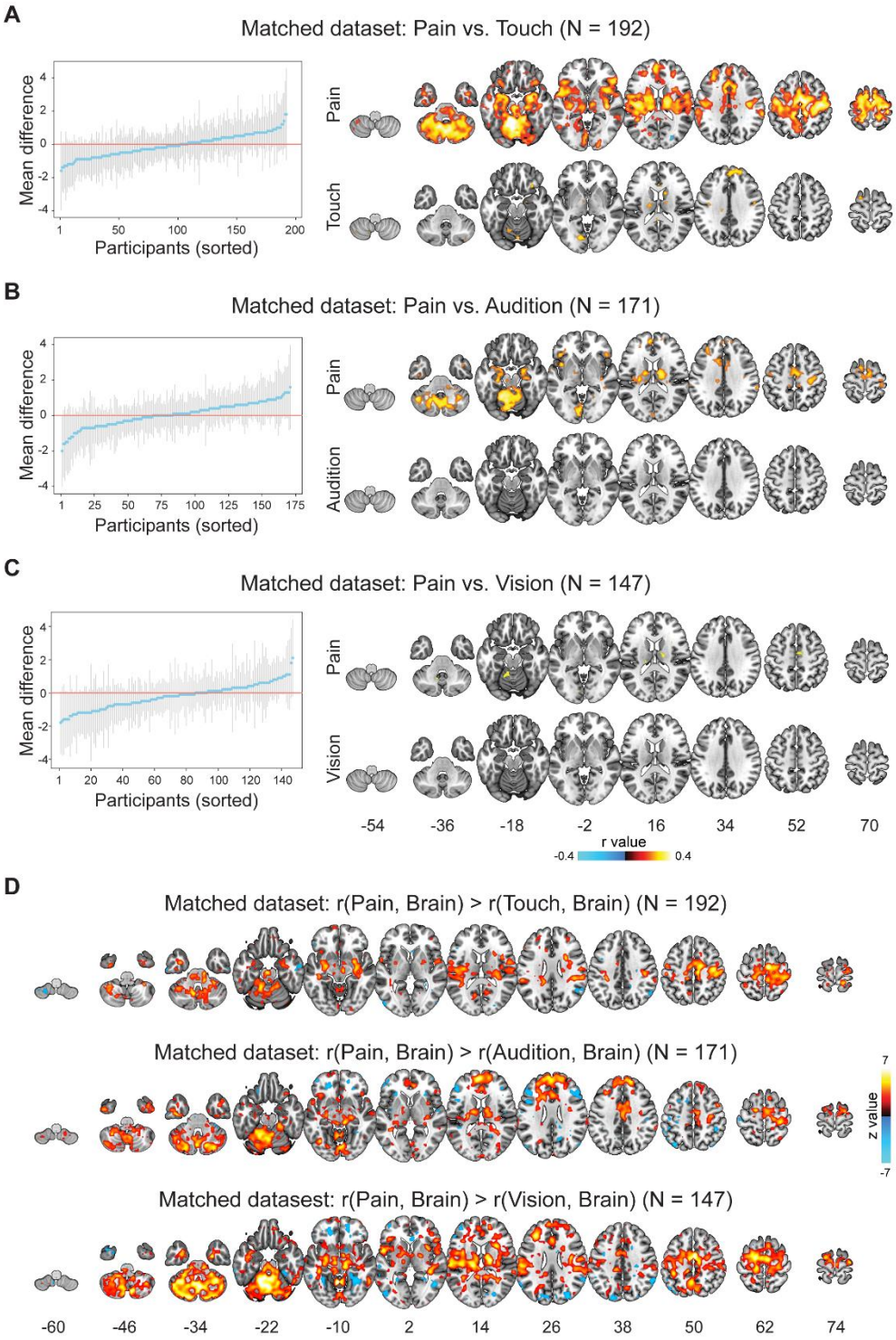

Figure 5. Correlation between BOLD responses and sensory sensitivity after sensitivity matching. (A)~(C) BOLD responses-sensory sensitivity correlation for pain and nonpain after sensitivity matching. In sensitivity matching, we selected participants whose mean pain and tactile (A), auditory (B), or visual (C) ratings did not differ

significantly. After the pain-touch and pain-audition matching, pain-evoked BOLD responses still correlated with pain sensitivity. After pain-vision matching, only a few areas showed a correlation with pain sensitivity. In contrast, far fewer areas correlated with tactile/auditory/visual sensitivity in all matchings. **(D)** Comparisons of BOLD-sensitivity correlation between pain and nonpain modalities after sensitivity matching. Direct comparisons of correlation coefficients showed larger correlations for pain than for touch, audition, and vision. Error bars in (A)~(C) stand for 95% confidence intervals for the rating differences for each participant.

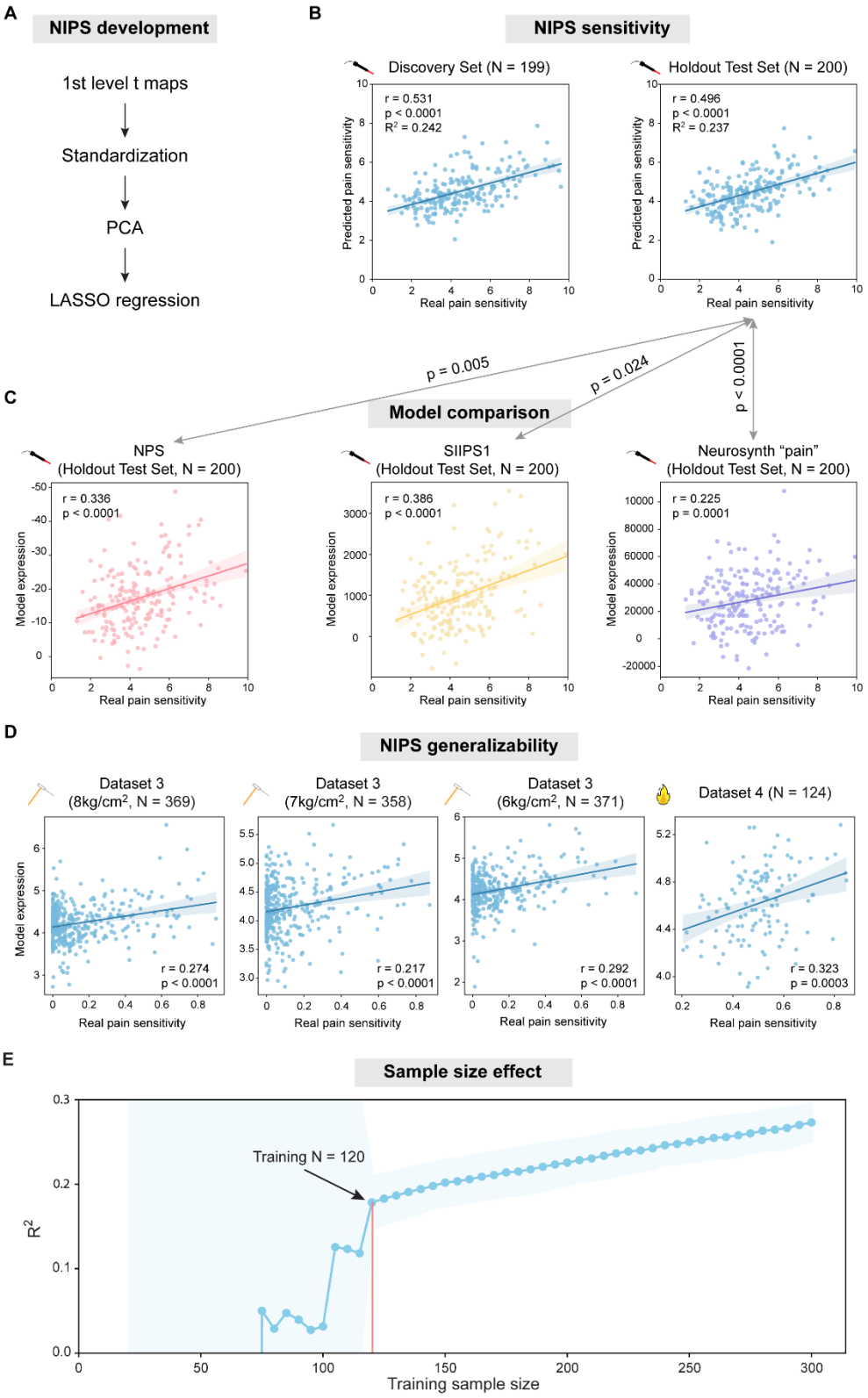

Figure 6. Development of NIPS and its performance. (A) Development of NIPS. We used first level t maps for pain as features and built our model (NIPS) with LASSO-PCR.

(B) Performance of NIPS in the Discovery Set and Holdout Test Set. In both datasets, NIPS showed good performance, explaining >20% of the variance of pain sensitivity. **(C)** Comparisons of NIPS and other models. Some well-established models performed not as well as NIPS, which was specifically developed to predict pain sensitivity with laser heat pain data. **(D)** Generalizability of NIPS. Although developed with laser heat pain data, NIPS significantly predicted mechanical and contact heat pain sensitivity in external datasets. **(E)** Effect of sample size on NIPS performance. NIPS's performance varied dramatically with small training sample sizes, but stabilized and continuously improved as training sample sizes exceeded 120. Shaded regions in (B)~(D) stand for 95% confidence intervals, and shaded regions in (E) represent standard deviation (SD) of R^2.

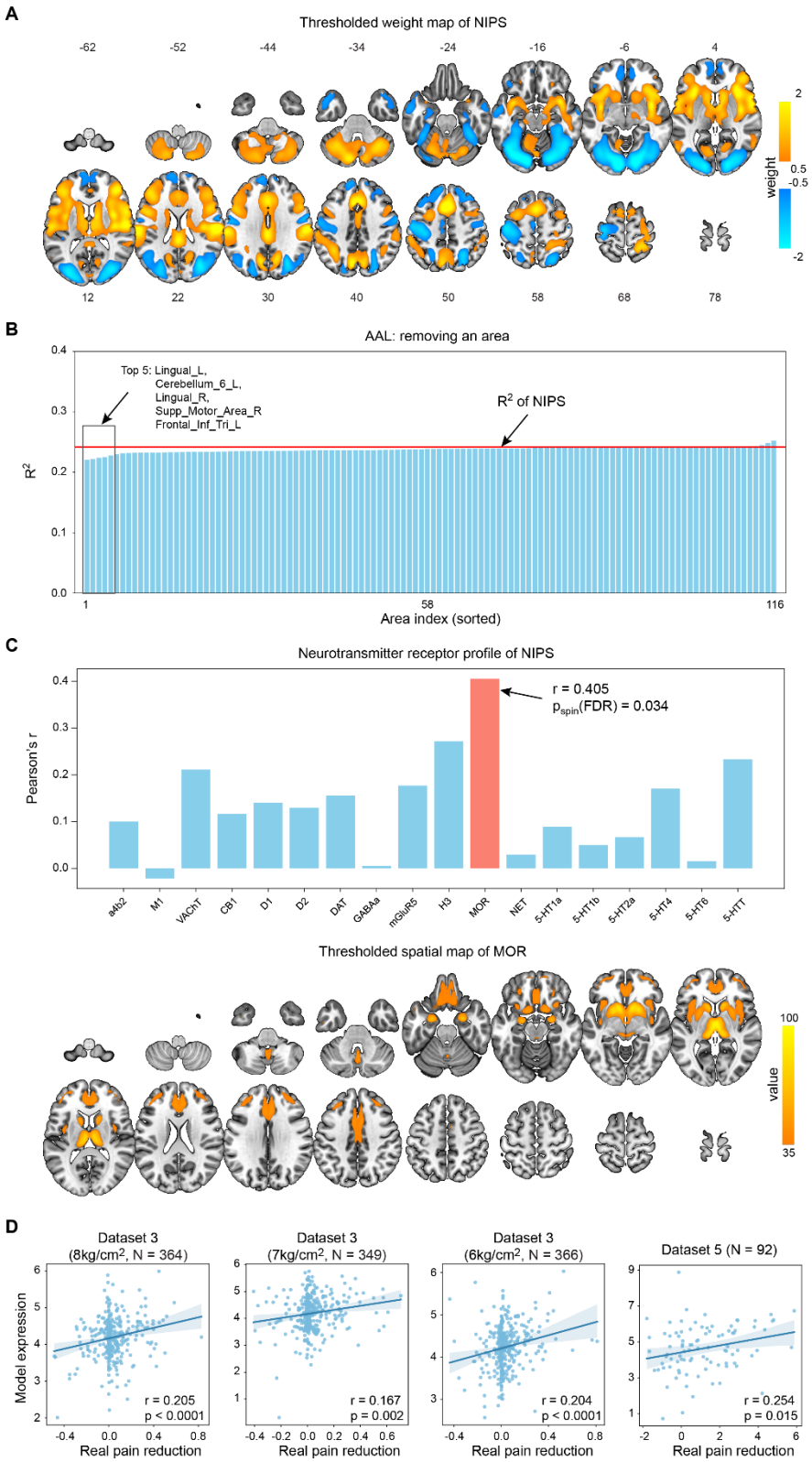

Figure 7. Interpretation of the weight map of NIPS. (A) Thresholded weight map of NIPS. For the sake of visualization, the weight map was thresholded at 0.5/-0.5 (p(FDR) <

0.05 for all surviving voxels). Model prediction was made with the unthresholded map. **(B)** Virtual lesion of NIPS. Removing brain regions one by one did not make NIPS's performance substantially worse, suggesting that a distributed network rather than isolated areas is responsible for encoding pain sensitivity. **(C)** Neurotransmitter profile of NIPS and thresholded spatial distribution of MOR. Assessed by the spin test, the weight map of NIPS correlated significantly with the spatial map of MOR. **(D)** Prediction of pain relief by NIPS. In Datasets 3&5, NIPS significantly predicted pain reduction after pain treatments. a4b2: alpha-4 beta-2 nicotinic receptor; M1: muscarinic acetylcholine receptor subtype M1; VAChT: vesicular acetylcholine transporter; CB1: cannabinoid type-1 receptor; D1: dopamine D1-type receptor; D2: dopamine D2-type receptor; DAT: respective dopamine transporter; mGluR5: metabotropic glutamate type 5 receptor; H3: histamine H3 receptors; MOR: μ-opioid receptor; NET: norepinephrine transporter; 5-HT1a: serotonin 1A receptor; 5-HTT: serotonin transporter. Shaded regions in (D) stand for 95% confidence intervals.